



The Effect of the Non-Newtonian Behavior of Blood on Capture Efficiency of Particles in a Vessel with a Local Symmetrical Stenosis

Ardalan Aram¹ · Aminan Saman^{1,2} · Lahonian Mansour¹

Accepted: 10 January 2024 / Published online: 27 January 2024

© The Author(s), under exclusive licence to Springer Science+Business Media, LLC, part of Springer Nature 2024

Abstract

Magnetic drug targeting (MDT) has garnered significant attention in the field of cancer treatment and other diseases due to its ability to minimize side effects and enhance treatment efficacy. This approach involves the injection of magnetic nanoparticles into the bloodstream, which are then guided to the tumor site through the application of an external magnetic field. In this particular study, the researchers focused on investigating the impact of various factors on the absorption of nanoparticles downstream of a stenosis in a vessel with local symmetric stenosis. Specifically, they examined the effects of the nanoparticles' diameter, Reynolds number, the Newtonian and non-Newtonian behavior of blood, magnetic field strength, and the type of magnetic field source. The two types of magnetic field sources considered were a current-carrying wire and a permanent magnet. The findings revealed that an increase in the nanoparticles' diameter and the magnetic field's strength led to an increase in the number of captured nanoparticles. Conversely, an increase in the Reynolds number resulted in a decrease in the captured nanoparticles. Additionally, the study highlighted the importance of considering blood as a non-Newtonian fluid for blood velocities lower than 60 mm/s (i.e., in arteries with a diameter lower than 2 mm). Furthermore, when comparing the efficiency of different magnetic fields, it was observed that the current-carrying wire was more effective for small-sized vessels with stenosis.

Keywords MDT · Nanoparticles · Stenosis · Current-carrying wire · Non-Newtonian

Abbreviations

u_l	Blood velocity (m/s)	B_n	Magnetic flux density (T)
u	X-component of blood velocity (m/s)	H	Magnetic field (T)
v	Y-component of blood velocity (m/s)	F_D	Drag force (N)
\bar{u}	Mean velocity (m/s)	C_D	Drag coefficient (1)
ρ	Blood density (kg/m ³)	a_1, a_2, a_3	Constants (1)
p	Blood pressure (Pa)	F_m	Magnetization force (N)
g	Gravitational acceleration constant (m/s ²)	M	Magnetization of materials (A/m)
μ	Blood viscosity (N s/m ²)	μ_0	Magnetic permeability of vacuum (H/m)
σ	Electrical conductivity of blood (S/m)	M_s	Saturation magnetization (A/m)
u_p	Particle velocity (m/s)	X_i	Natural magnetic susceptibility (1)
Re_p	Reynolds number of particles (1)	X_{eff}	Effective magnetic susceptibility for spherical particles (1)
ρ_p	Particles' density (kg/m ³)	I	Electric current (A)
d_b	Particles' diameter (m)	s	Distance between the desired point and current-carrying wire (m)
		n_t	Total number of particles
		n_{ROI}	Captured particles at region of interest(ROI)

✉ Lahonian Mansour
mlahonian@uok.ac.ir

¹ Department of Mechanical Engineering, University of Kurdistan, Sanandaj, Iran

² Department of Mechanics, Electrical Power and Computer, Science and Research Branch, Islamic Azad University, Tehran, Iran

1 Introduction

Researchers have long been concerned with improving the effectiveness of drugs while minimizing their side effects in the treatment of diseases. Traditional therapies, such as oral or intravenous injections, often result in a significant portion of the drug being distributed throughout the body instead of reaching the intended target tissue. This widespread distribution can lead to unwanted side effects for the patient. However, in recent years, magnetic drug targeting (MDT) has emerged as a promising approach to address this issue. MDT involves the injection of magnetic nanoparticles into the bloodstream, upstream of the target tissue. These nanoparticles are then attracted to the tumor site using an external magnetic field. Once at the target tissue, the nanoparticles are released and the magnetic field is removed. As a result, the nanoparticles are repelled from the body, ensuring that they do not cause any specific side effects [1–3].

The reason for using magnetic nanoparticles (MNPs) for targeting purposes is based on their ability to minimize or eliminate the adverse effects caused by chemotherapy drugs. This objective is achieved by reducing their widespread distribution in the body and enabling the precise delivery of lower doses of cytotoxic substances used in these therapies. Moreover, MNPs exhibit potential for various applications in the field of biomedicine, such as bioseparation and magnetic resonance imaging (MRI) [4–6]. There are various methods available for the synthesis of magnetic nanoparticles used in drug delivery applications. These nanoparticles usually comprise of a magnetic iron oxide core, commonly known as magnetite (Fe_3O_4) or maghemite ($\gamma\text{-Fe}_2\text{O}_3$), and a polymer shell made of dextran [7]. Moreover, scientific evidence has demonstrated that the application of a magnetic coating on nanoparticles effectively inhibits their aggregation within a liquid medium. This not only enhances their chemical stability but also offers superior protection against potential toxicity [8]. One instance of a novel type of coating is the double surfactant coating, which exhibits remarkable biocompatibility for MNPs, thereby rendering them highly promising for clinical applications [9].

Rotariu and Strachan [10] conducted a study to evaluate the delivery of magnetic nanoparticles to a tumor. Their findings revealed that when the size of the magnet was sufficiently large, nanoparticles with a diameter of less than 1 μm exhibited high capture rates. Conversely, in cases where the tumor was large, the magnetic field source needed to be positioned farther away, requiring a larger region of interest (ROI) to effectively capture the desired number of nanoparticles. In a separate study, Furlani [11] investigated the movement of nanoparticles in blood flow under

the influence of a permanent magnet. The study focused on the impact of the distance between the magnet center and the vessel center. It was observed that as this distance increased, the capture of nanoparticles at the vessel wall decreased. Sharma et al. [12] investigated the trajectory of magnetic nanoparticle displacement within a microvessel subjected to a magnetic field generated by a permanent magnet. Their findings underscored the pronounced impact of the spatial separation between the magnet and the transverse section of the vessel, demonstrating a consequential influence on the nanoparticles' capture locations. Habibi et al. [13] numerically investigated the concentration of magnetic nanoparticles in a non-Newtonian fluid under the influence of an external magnetic field. The study revealed changes in flow and pressure fields, highlighting the distance from the magnetic field and the radius of nanoparticles as two significant parameters. Furthermore, Habibi et al. [14] examined the distribution of nanoparticles in a pulsed blood flow near a magnetic field. They observed that during heart pumping, the sudden increase in blood flow velocity and the overcoming of drag force allowed nanoparticles to pass through the magnetic field. Additionally, with increasing injection time, the shear stress on the vessel wall decreased, leading to longer nanoparticle retention time in the blood flow. Stuart et al. [15] explored the capture of nanoparticles in curved vessels using four different modes of magnetic field generated by a conductive wire at the bending region. The study aimed to identify the optimal location of the current-carrying wire to enhance nanoparticle capture. In a related study, Sharma et al. [16] scrutinized the velocity field of a bio-magnetic fluid within a vessel, exposing it to uniform magnetic fields at varying Hartmann numbers. The outcomes revealed a discernible reduction in fluid velocity at the vessel's center with escalating Hartmann numbers. Furthermore, Shazri and Idres [17] analyzed the course of nanoparticle movement within microvessels of distinct diameters when exposed to a magnetic field generated by a magnet. Their investigation involved calculating the nanoparticle capture under diverse conditions, including different nanoparticle diameters and varying distances between the magnet and the vessel. Bose and Banerjee [18] conducted an investigation into the entrapment of nanoparticles within a three-dimensional vessel characterized by curvature and stenosis, considering non-Newtonian blood flow across four distinct models and locations for the current-carrying wire. The study adopted blood as a non-Newtonian fluid, exploring four distinct non-Newtonian models for blood flow. The optimal positioning of the current-carrying wire, serving as a magnetic field source, was delineated to enhance particle capture within the specified region of interest (ROI). Additionally, the study discerned regions particularly susceptible

to restenosis. Türk et al. [19] examined the flow dynamics of a bio-magnetic fluid within a vessel featuring diverse stenosis configurations under the influence of an external magnetic field. The research identified a substantial impact on the flow field when the magnetic field source was positioned downstream of a larger stenosis. Furthermore, augmenting field strength in both horizontal and vertical directions was associated with increased vortex size induced by stenosis, directing the flow towards the upper wall and elevating temperature. In a separate study, Bose and Banerjee [20] scrutinized the capture of magnetic nanoparticles by a current-carrying wire across various Reynolds numbers and magnetic field strengths, considering Newtonian blood flow within a vessel exhibiting stenosis and bifurcation. Their findings underscored the intricate interplay of magnetic field strength, flow velocity, and nanoparticle diameter in influencing capture. Barnsley et al. [21] numerically and experimentally explored the capture and trajectory of nanoparticles within vessels featuring stenosis and those devoid of stenosis under the influence of a magnetic field generated by a Halbach array of permanent magnets. The study revealed that the morphology and angle of the permanent magnet, fluid flow velocity, and the presence of stenosis exerted significant influence on nanoparticle capture. Victor et al. [22] conducted an empirical study utilizing nanoparticles to examine the impact of a magnetic field on the passage of micro-sized bubbles through a bifurcated vessel, one branch of which was obstructed. Their findings demonstrated the feasibility of drug delivery to obstructed vessels through the application of a magnetic field. Alizadeh et al. [23] focused on the impact of injection angle and rate on capture efficiency (CE) in a three-dimensional blood vessel. Three magnetic sources were considered: a permanent magnet, a current-carrying wire, and a coil wire. Results showed the current-carrying wire had the highest CE (94%), followed by the permanent magnet (80%) and the coil wire (68%). The maximum CE of nanoparticles (91.7%) in scenario 2 was achieved at an injection rate of $31.4 \text{ mm}^3 \text{ s}^{-1}$ with the current-carrying wire. No particles were captured in scenario 1 for injection rates from 0 to $62.8 \text{ mm}^3 \text{ s}^{-1}$.

Manshadi et al. [24] investigated the capture of nanoparticles and their trajectory within a vessel characterized by four-layer porous walls and asymmetric stenosis replacing a conventional stenotic region. This investigation employed a permanent magnet, and the researchers explored the influence of factors such as magnetic field size, magnet dimensions, particle diameter, initial particle location, and the relative magnetic permeability of particles on particle capture. The study's outcomes revealed that an escalation in particle size, relative magnetic permeability, proximity to the upper wall, as well as magnetic field strength and magnet dimensions collectively contributed to an increased capture of nanoparticles within

the porous wall. The presence of stenosis further intensified particle uptake in this area, accompanied by vein constriction. Lahonian et al. [25] investigated the capture efficiency (CE) of magnetic carrier particles in a micro-vessel at the region of interest (ROI). A nonuniform magnetic field generated by a Nd-Fe-B magnet was used to capture the carrier particles at the ROI. The study considered interactions between particle-particle and red blood cell (RBC)-carrier particle, as well as factors such as carrier particle diameter, magnetic force, and the non-Newtonian behavior of blood. The governing equations were solved using the finite element method. Four scenarios were analyzed: (1) Newtonian fluid without interaction forces, (2) Newtonian fluid with interaction forces, (3) non-Newtonian fluid without interaction forces, and (4) non-Newtonian fluid with interaction forces. The results showed that for a particle diameter of 2000 nm, the CE values were 70% and 53% for the cases without and with interaction forces, respectively. Considering the interactions between particle-particle and RBC-carrier particle led to an average decrease of nearly 19% in the CE of carrier particles for all magnet-vessel distances. At a magnet-vessel distance of 2.5 cm, the CE values for case 2 and case 3 were approximately 70% and 45%, respectively, representing the maximum and minimum CE values. Notwithstanding preceding research efforts, it is evident that a comprehensive examination of nanoparticle capture downstream of a vessel with stenosis, encompassing diverse Reynolds numbers, nanoparticle diameters, magnetic field strengths, non-Newtonian behavior of blood, and types of magnets employed (namely, current wire and permanent magnet), has yet to be adequately addressed.

The current investigation examines the impact of various factors, including the Reynolds number, particle diameter, magnetic field strength, and different magnetic field sources (specifically, cylindrical permanent magnets and current-carrying wires), on the CE of particles in a non-Newtonian blood regime downstream of a stenosis in a 2D cylindrical blood vessel. The study focuses on a symmetric stenosis and positions a magnet in the region of interest (ROI) after the stenosis. The findings indicate that the CE at the ROI is influenced by the Reynolds number, magnetic field strength, and particle diameter. Additionally, the stenosis significantly affects the motion of particles and consequently has a substantial impact on their CE downstream of the stenosis. Furthermore, the results highlight the importance of considering blood as a non-Newtonian fluid, particularly for blood velocities below 60 mm/s (i.e., in arteries with a diameter below 2 mm).

2 Model Description

The finite element method (FEM) was employed in this research to examine the movement of nanoparticles within a vessel that has stenosis. These nanoparticles are introduced

into a blood vessel with specific dimensions, including a diameter (D) and length (L). The blood flow occurs in the X-direction. To exert a magnetic force, a rare-earth cylindrical magnet is utilized, while the current-carrying wire is positioned at an undisclosed location. Figure 1 illustrates a schematic representation of the geometry being investigated in this study.

2.1 Stenosis Geometry

As shown in Fig. 1, there is symmetrical stenosis in the vessel. The upper and lower walls of the vessel are obtained from the following formulas [26]:

$$y_{lower} = A_1 \operatorname{sech}(B_1(x - x_1)) \quad (1)$$

$$y_{upper} = 0.2 - A_2 \operatorname{sech}(B_2(x - x_2)) \quad (2)$$

where A_1 and A_2 are positive constants ($A_1 = A_2 = 0.065$) controlling the degree of constriction, B_1 and B_2 are constants ($B_1 = B_2 = 10$) that control the length of the occluded area, and x_1 and x_2 denote the location of throat of stenosis ($x_1 = x_2 = 1.5$).

In this study, D and L are 0.002 m and 0.04 m, respectively, and the stenosis is considered far enough from the inlet. CE is a ratio showing the number of particles captured in the RIO to the total particles, where the ROI is defined as $x_{wire} - 2D \leq ROI \leq x_{wire} + 2D$.

2.2 Formulation

A laminar, incompressible, and fully developed flow has been considered in the blood vessel. The drug carrier nanoparticles are uniformly distributed at the inlet, and the particle-particle interaction has been neglected. By performing the dimensional analysis and based on the assumptions made, blood flow can be considered as steady state [20, 26,

27]. Therefore, governing equations of the fluid phase are as follows:

2.2.1 Fluid Phase

The continuity equation is as follows:

$$\frac{\partial u}{\partial x} + \frac{\partial v}{\partial y} = 0 \quad (3)$$

The momentum equation is as follows:

$$\rho \left(u \frac{\partial u}{\partial x} + v \frac{\partial u}{\partial y} \right) = -\frac{\partial p}{\partial x} + (J \times B_n)_x + \mu \left(\frac{\partial^2 u}{\partial x^2} + \frac{\partial^2 u}{\partial y^2} \right) \quad (4)$$

where $J \equiv (J_x, J_y)$ is the current velocity, $B_n = (B_x, B_y)_n$ is the magnetic flux density, in which B_1 , denoting the current-carrying wire's magnetic flux density and B_2 is for permanent magnet's magnetic flux density, and σ is the electric conductivity. Assume that $E \equiv E_x, E_y = (E_x, 0)$ denotes the electric field. From Ohm's law:

$$J_x = \sigma(E_x + uB_x), J_y = 0 \quad (5)$$

In the case of the steady flow, Maxwell's equation $\nabla \times E = 0$ implies that E_z is constant. For the present study, we assume that E_z is zero. Then, $J_x = -\sigma u B_x^2 A$; therefore, $J \times B = -\sigma u B_x^2$. Hence, Eqs. (4) and (5) become [28] as follows:

$$\rho \left(u \frac{\partial u}{\partial x} + v \frac{\partial u}{\partial y} \right) = -\frac{\partial p}{\partial x} - (\sigma B_n^2 u)_x + \mu \left(\frac{\partial^2 u}{\partial x^2} + \frac{\partial^2 u}{\partial y^2} \right) \quad (6)$$

$$\rho \left(u \frac{\partial v}{\partial x} + v \frac{\partial v}{\partial y} \right) = -\frac{\partial p}{\partial y} + \mu \left(\frac{\partial^2 v}{\partial x^2} + \frac{\partial^2 v}{\partial y^2} \right) \quad (7)$$

where the term $-\sigma B_n^2 u$ is the Lorentz force. Lorentz force arises due to the electric current generated from the moving electrically conductive fluid within a magnetic field.

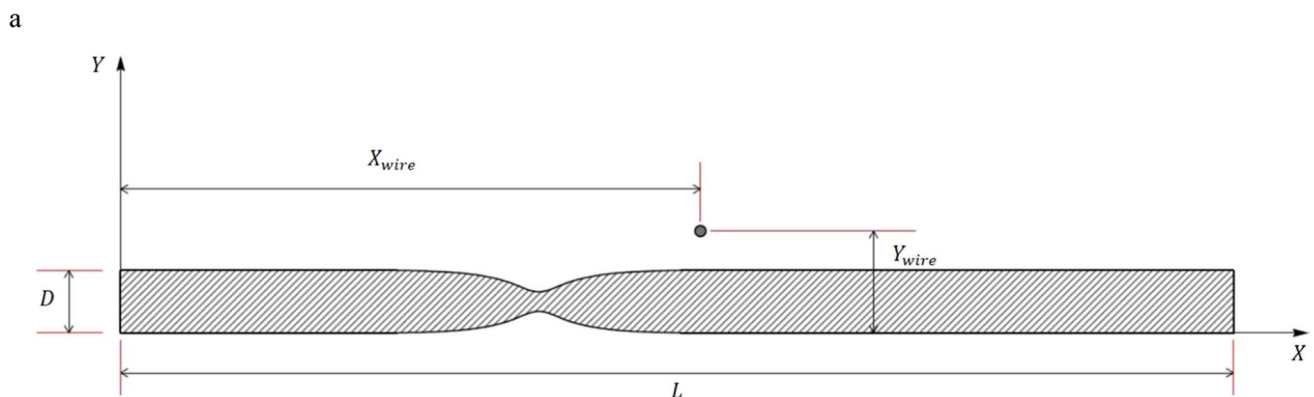


Fig. 1 Schematic of the geometry of the present study

Plasma has moving ions so that blood can be considered as an electrically conductive fluid; considering the fact that blood velocity in the Y-direction is not considerable, we can eliminate Lorentz force in this direction [20, 26, 29].

For non-Newtonian blood, the Carreau model is used [20]:

$$\mu = \mu_\infty + (\mu_0 - \mu_\infty) [1 + (\lambda \dot{\gamma})^2]^{\frac{n-1}{2}}, \quad \dot{\gamma} = \frac{\bar{u}}{D} \tag{8}$$

where $\mu_0 = 0.056$ Pa s, $\mu_\infty = 0.0032$ Pa s, $\lambda = 3.131$ s, and $n = 0.3568$.

The fully developed velocity profile is given as follows:

$$\frac{u}{\bar{u}} = 1.5 \left(1 - \left(\left(\frac{2y}{D} \right) - 1 \right)^2 \right) \tag{9}$$

where D is the diameter of the vessel. The boundary conditions of the problem are as follows:

$$u = v = 0 \begin{cases} y = y_{lower}, & 0 \leq x \leq L \\ y = y_{upper}, & 0 \leq x \leq L \end{cases}$$

$$\frac{\partial u}{\partial y} = 0 \quad y = \frac{D}{2}, \quad 0 \leq x \leq L \tag{10}$$

2.2.2 Nanoparticle Phase

Several forces acted on the particle in MDT, including drag force, magnetic force, thermophoretic force, particle-particle interaction, and buoyancy force. In the present work, magnetic force, buoyancy force, and drag force were considered.

The motion of nanoparticle in a vessel is governed by using Newton’s second law:

$$\sum F = \frac{du_p}{dt} \tag{11}$$

where F includes drag, buoyancy, and magnetic force.

Drag Force Since the volume fraction of nanoparticles is very low (of order 10^{-6}), hence, the effect of the dispersed phase in the fluid is negligible [30]. So one-way coupling is sufficient, and only the drag force applied on the nanoparticles is included. In order to calculate drag force acting on the particle, the following formulas are used [31]:

$$F_D = \frac{3\mu C_D Re_p}{4\rho_p d_p^2} (u_b - u_p) \tag{12}$$

$$Re_p = \frac{\rho |u_b - u_p| d_p}{\mu} \tag{13}$$

where u_b is the blood velocity, Re_p is Reynolds number of particles, and C_D is the drag coefficient, which is defined by $C_1, C_2,$ and C_3 constants and Re_p as follows:

$$C_D = C_1 + \frac{C_2}{Re_p} + \frac{C_3}{Re_p^2} \tag{14}$$

Buoyancy Force Buoyancy arises from the fact that fluid pressure increases with depth, and the increased pressure is exerted in all directions (Pascal’s principle) so that there is an unbalanced upward force on the bottom of a submerged object. The buoyancy force is calculated as follows [20]:

$$F_G = \frac{g(\rho_p - \rho_b)}{\rho_p} \tag{15}$$

Magnetic Force The magnetic force acting on a particle of volume V , known as magnetophoretic force, is calculated by [20]:

$$F_M = \iiint \mu_0 M \cdot \nabla H dV \tag{16}$$

where H is the magnetic field, and M is the magnetization of materials. For magnetic fields more than a specific limit, it reaches its critical value, M_s , which results in the following formula:

$$M = \begin{cases} X_{eff} & H < \frac{M_s}{X_{eff}} \\ M_s & H \geq \frac{M_s}{X_{eff}} \end{cases} \tag{17}$$

X_{eff} is the effective magnetic susceptibility. For a spherical particle, the effective magnetic susceptibility is related to natural magnetic susceptibility via this relation:

$$X_{eff} = \frac{3X_i}{(3 + X_i)} \tag{18}$$

In the present study, by considering $x_i \gg 1$, it was assumed that $X_{eff} \approx 3$.

For a curl-free magnetic field, Eq. (17) becomes

$$F_M = \begin{cases} \mu_0 \frac{\pi d_p^3}{2} (H \cdot \nabla) H & H < \frac{M_s}{3} \\ \mu_0 \frac{\pi d_p^3}{2} M_s \nabla H & H \geq \frac{M_s}{3} \end{cases} \tag{19}$$

For a current-carrying wire, the amount of field at each point can be obtained as follows [18]:

$$H = \frac{I}{2\pi s} \tag{20}$$

where s is the distance between the desired point and the current-carrying wire.

The capture efficiency (CE) is defined as the ratio of the particles captured at ROI to the total number of particles [32, 33]:

$$CE = \frac{n_{in} - n_{out}}{n_{in}} \quad (21)$$

where n_{in} and n_{out} are the total number of carrier particles and the particles that are not captured, respectively.

3 Results and Discussion

3.1 Grid Independence

The investigation of the grid independence in relation to the particles located at the upper wall of the vessel at the region of interest (ROI) was conducted to ensure accuracy. This study focused on a scenario where the magnetic field strength was set at 1.0 T at the coordinates (2, 0.1), the Reynolds number was 100, and the diameter of the particles was 1000 nm. It is important to note that a total of 1000 nanoparticles were utilized for this particular investigation. The results depicted in Fig. 2 illustrate the percentage of computational efficiency (CE) for various mesh numbers. The figure reveals that there is a marginal increase of 0.01% in CE when the number of meshes is increased from 36,000 to 50,000. Consequently, a total of 36,477 elements were employed for further analysis, as it was deemed sufficient for accurate calculations.

3.2 Validation

The validation of the present work divides into two parts. First, the magnetic field produced by the current-carrying wire and the permanent magnet was validated. In the second part, the motion of the nanoparticles within the blood flow was validated.

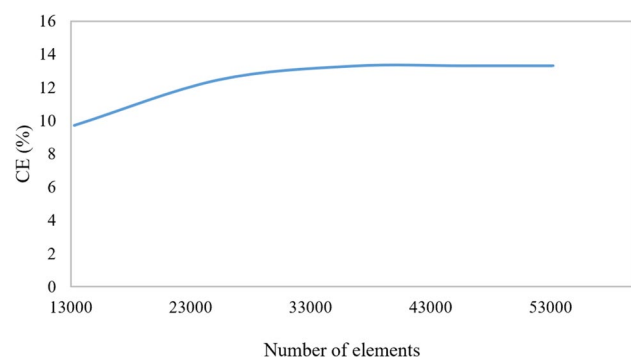


Fig. 2 Grid independency

3.2.1 Magnetic Field

The validation process in this section focused on confirming the magnetic field generated by the current-carrying wire and the cylindrical permanent magnet. The magnetic flux density (B) produced by the cylindrical permanent magnet in our study was compared to the experimental findings of Camacho et al. [34], as illustrated in Fig. 3. The distance from the surface of the cylindrical magnet, denoted as “Z,” was taken into consideration. It is evident from the figure that as the distance between the magnet and the vessel increases, the strength of the magnetic field decreases. These results align well with the experimental outcomes presented by Camacho et al. [34]. The outward-directed magnetic field is generated by a current-carrying wire that is perpendicular to the X-Y plane. In order to validate the findings, the obtained results were compared to the calculated results derived from Eq. (20) [18]. Table 1 presents the magnetic field norm resulting from the current-carrying wire, along with the values obtained from Eq. (20). The current flowing through the wire is 1×10^4 amps. The analysis reveals that the maximum error rate for this particular aspect is 1%, indicating a high level of agreement between the results.

3.2.2 Motion of Nanoparticles

In Fig. 4, the trajectory of a particle released from the center of the vessel in the current study is compared to the

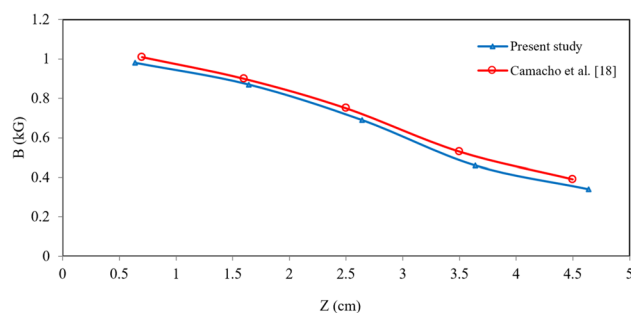


Fig. 3 Comparison of the magnetic flux density (B) between the present study and Camacho et al. [34]

Table 1 Comparison of magnetic field norm produced by current-carrying wire with calculated results from Eq. (20)

Distance from the wire (cm)	Magnetic field norm (A/m) from Eq. (20)	Magnetic field norm (A/m) for present study
1	1591.55	1588
2	795.77	791
3	530.5	527
4	397.88	394

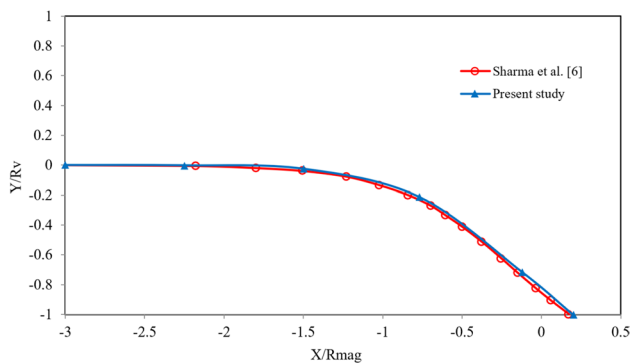


Fig. 4 Comparison of the trajectory of a particle released from the center of the vessel for $d = 3.5$ cm for the present study with Sharma et al. [12]

Table 2 Physical properties of blood and nanoparticles

Parameter	Value
ρ_b (kg/m ³)	1060
μ_0 (N s/m ²)	0.0032
σ (S/m)	0.8
ρ_p (kg/m ³)	5000
M_s (A/m)	10 ⁶
d_p (nm)	500–2000

trajectories of Sharma et al. [12]. The distance between the center of the vessel and the center of the permanent magnet is 3.5 cm. The figure clearly shows that when the particle is in the range of $(-3 \leq x/R_{mag} \leq -1)$, it follows a straight path due to the weak magnetic field in this region. However, as the particle approaches the magnet location $(-1 \leq x/R_{mag} \leq 1)$, it experiences a strong magnetic force, causing a change in its direction. Eventually, the particle is captured at the location of $(x/R_{mag} = 0.2)$, just after the peak of the magnetic field at the center of the magnet.

3.3 Effect of Parameters on CE

3.3.1 Reynolds Number

Table 2 shows the parameters of blood and particles used in the present study. In Fig. 5, the effects of particles' diameter on the CE of nanoparticles at different Reynolds number under the magnetic field of 1 T produced by the current-carrying wire are shown. Particles with larger sizes contributed to the higher CE. The increase in particle sizes up to 2000 nm resulted in the CE enhancement of 9.5% and 4.8% at Reynolds number of 50 and 100, respectively. The higher CE is attributed to the lower drag force at $Re = 50$, where the

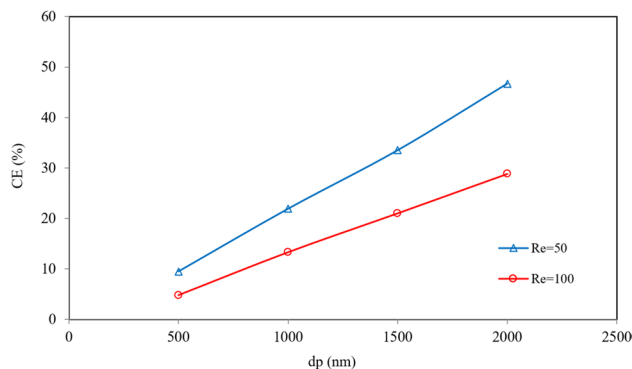


Fig. 5 CE of nanoparticle for various particle diameters and $Re = 50$ and $Re = 100$

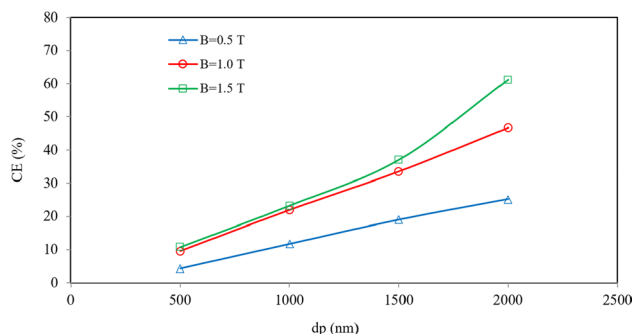


Fig. 6 CE of nanoparticle for different particle diameters and different magnetic fields at $Re = 50$

magnetic force becomes more effective, resulting in more particles being captured at ROI.

The findings additionally indicated that the CE exhibited a higher value when compared to across the entire spectrum of particle sizes. The study revealed that as the diameter of the particles increased, the difference in CE for two Reynolds number also increased. For instance, when the particle diameter was 500 nm, the CE difference between $Re = 50$ and $Re = 100$ was 4.7%, whereas for a particle diameter of 2000 nm, this difference escalated to 17.9%.

3.3.2 Magnetic Field

In Figs. 6 and 7, the CE variations of nanoparticles with different diameters and magnetic fields of 0.5, 1, and 1.5 T in $Re = 50$ and $Re = 100$ are depicted. Both figures demonstrate that an increase in magnetic field strength leads to an increase in the CE of the particles across all particle diameters. Specifically, the CE of the particles is higher when the magnetic field is increased from 0.5 to 1 T compared to when it is increased from 1 to 1.5

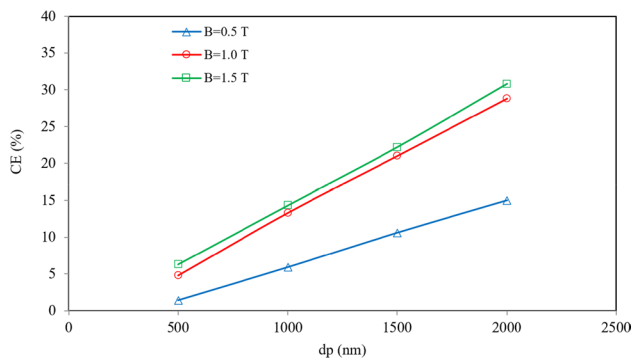


Fig. 7 CE of nanoparticle for different particle diameters and different magnetic fields at $Re = 100$

T. This discrepancy can be attributed to the fact that a significant number of particles are captured before reaching the region of interest (ROI) when the magnetic field is increased from 1 to 1.5 T. It is important to note that particles not captured in the ROI are not included in the CE calculation. Consequently, it can be concluded that for particle diameters less than 1500 nm, increasing the magnetic field from 1 to 1.5 T has a negligible effect on CE (approximately 1.5%). However, for particle diameters greater than 1500 nm, increasing the magnetic field from 1 to 1.5 T has a substantial effect on CE (approximately 14.5%). The magnetic fields of 0.5, 1, and 1.5 T were generated using currents of 5000, 10,000, and 15,000 amps, respectively, in the current-carrying wire. It is worth mentioning that in this particular section, the stenosis is assumed to be symmetric and equal to 65%.

In Fig. 7, a similar pattern to Fig. 6 is observed for $Re = 100$. However, the only distinction between the trends of these two figures is associated with the behavior of $B = 1.5$ T when the d_p is increased from 1500 to 2000 nm. The primary reason for this discrepancy is that at $Re = 50$, the drag force is relatively low. Consequently, when the magnetic field is increased to 1.5 T, its strength prevents the nanoparticles from passing through. As a result, a majority of the particles are captured at the ROI. On the other hand, in the case of $Re = 100$, the drag force is higher. Therefore, with an increase in the magnetic field, more particles are captured. However, due to the increased drag force, these particles do not have sufficient time to be captured, unlike the scenario with $Re = 50$. From these observations, it can be inferred that when particles have a larger diameter, the impact of an increased magnetic field on the CE is more pronounced compared to particles with a smaller diameter. This can be attributed to the significant influence of the particles' diameter on the magnetic force, as indicated by Eq. (19), where the magnetic force is a function of d^3 .

3.3.3 Non-Newtonian Behavior

The investigation in this section focuses on the non-Newtonian characteristics of blood. To represent blood as a non-Newtonian fluid, the Carreau model was employed. Figure 8 illustrates the comparison of the CE with varying diameters in both Newtonian and non-Newtonian blood fluids. It is important to note that the magnetic field strength remains constant at 1 T, and the average velocity of blood is consistent at 151 mm/s for both scenarios.

The figure presented in Fig. 8 illustrates that the CE is slightly lower for the non-Newtonian case compared to the Newtonian case. This decrease in CE can be attributed to the higher blood viscosity observed in the non-Newtonian case, which consequently leads to an increase in drag force (Fig. 9). As a result, the particles experience a greater drag force in the X-direction, ultimately resulting in a lower CE for this particular case. It is important to note that the drag force in the non-Newtonian case consistently surpasses that of the Newtonian case throughout the entire duration depicted in the Fig. 9. Furthermore, it is noteworthy that the difference in drag force between the two cases remains relatively constant over time. This explains why both plots in Fig. 8 exhibit a similar trend, albeit with varying values.

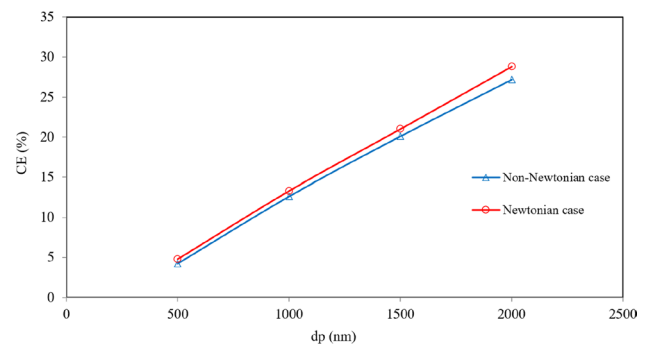


Fig. 8 CE of nanoparticle for different particle diameters at $B = 1$ T, $\bar{u} = 151$ mm/s

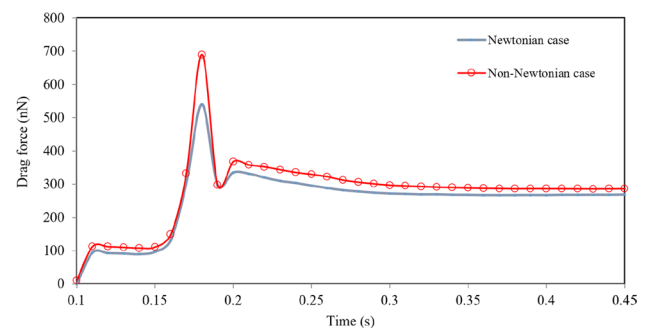


Fig. 9 Drag force on a particle released from the center of the vessel in Newtonian and non-Newtonian cases

Figure 10 illustrates the impact of both non-Newtonian and Newtonian models on the CE of nanoparticles. The parameters used in this study are $B = 1$ T and $d_p = 2000$ nm. When the average velocity (\bar{u}) is 75.5 mm/s, the CE is 37.6% for the non-Newtonian case and 47.6% for the Newtonian case. However, when \bar{u} increases to 151 mm/s, the CE decreases to 27.3% for the non-Newtonian case and 28.8% for the Newtonian case. The results clearly indicate that the difference in CE is much larger at $\bar{u} = 75.5$ mm/s compared to $\bar{u} = 151$ mm/s. This can be attributed to the fact that at $\bar{u} = 75.5$ mm/s, the shear rate (γ) is lower, resulting in a greater difference in viscosity between the Newtonian and non-Newtonian cases compared to $\bar{u} = 151$ mm/s. Consequently, the difference in drag force between the Newtonian and non-Newtonian cases is greater at $\bar{u} = 75.5$ mm/s, leading to a larger difference in CE.

In addition, it should be noted that the current state of the body’s arteries and the ratio of velocity to diameter in vessels with a diameter smaller than 2 mm (where the blood velocity is less than 60 mm/s) results in a strain rate of less than 100 s^{-1} . Therefore, the significance of the non-Newtonian characteristics of the blood and its impact on the capture efficiency of nanoparticles cannot be disregarded [20].

3.3.4 Magnet Type

Figure 11 illustrates the impact of magnet type, specifically permanent magnets and current-carrying wires, on the magnetic field component and the capture efficiency (CE) of nanoparticles. The measurements were taken at the center of the vessel, with a magnetic field strength (B) of 0.5 T, a particle diameter (d_p) of 1500 nm, and a Reynolds number (Re) of 100. The figure clearly demonstrates that the Y-component of the magnetic field generated by the permanent magnet is greater than that produced by the current-carrying wire. Consequently, a larger number of particles are captured before reaching the region of interest (ROI). In terms of quantitative analysis, the number of particles captured before the ROI varies depending on the magnetization direction of

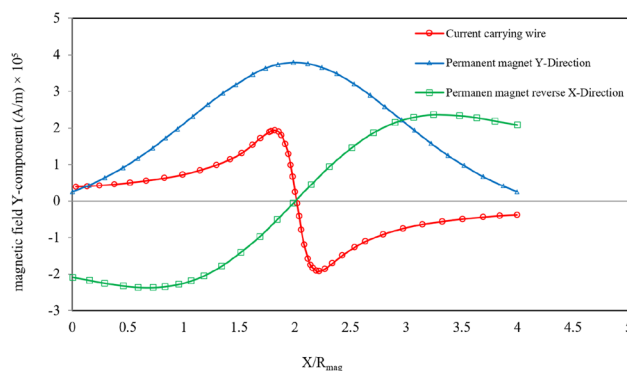


Fig. 11 Y-component of magnetic field for current-carrying wire and permanent magnet (with magnetization at reverse X and Y direction)

the permanent magnet, with values of 16, 310, and 372 for magnetization in the reverse X-direction, Y-direction, and both X and Y-directions, respectively. This ultimately leads to a lower CE at the ROI. Conversely, the magnetic gradient of the current-carrying wire is significantly higher at the ROI compared to other regions, particularly the stenosed region. As a result, fewer particles are captured before reaching the ROI. However, once the particles reach the ROI, they experience a peak in the magnetic field, leading to their capture. Consequently, it is anticipated that the CE of particles in the case of the current-carrying wire will be more significant compared to the permanent magnet, as depicted in Fig. 12.

3.4 Nanoparticles’ Velocity

This section focuses on the velocity of a nanoparticle that is released from the center of the vessel. In Fig. 13, the velocity variations of the nanoparticle are depicted for both Newtonian and non-Newtonian models. It is evident from the figure that in both models, the particle reaches stenosis at 0.15 s, resulting in a sharp increase in its velocity. The maximum velocity values observed in the throat for the Newtonian and

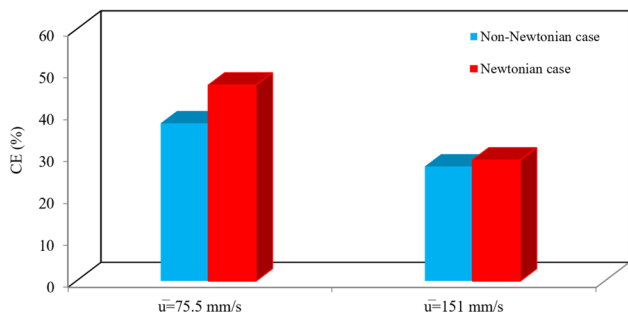


Fig. 10 The effect of non-Newtonian and Newtonian models on CE for $\bar{u} = 75.5$ mm/s and $\bar{u} = 151$ mm/s

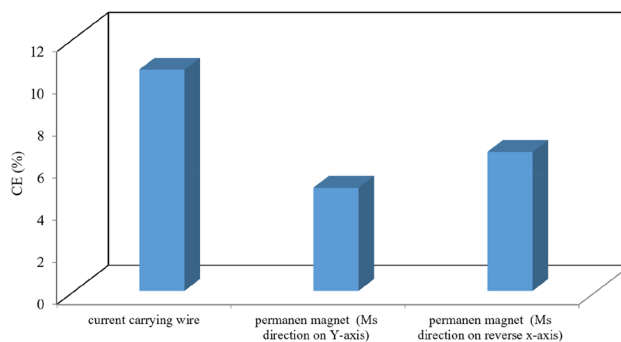


Fig. 12 CE of nanoparticles for permanent magnet and current-carrying wire magnetic fields

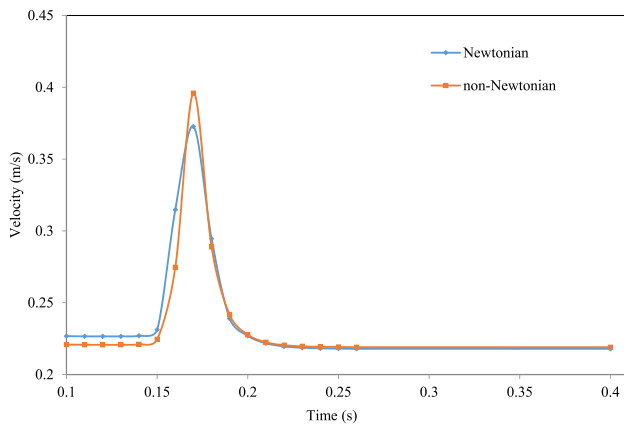


Fig. 13 Particle velocity for Newtonian and non-Newtonian models in terms of time

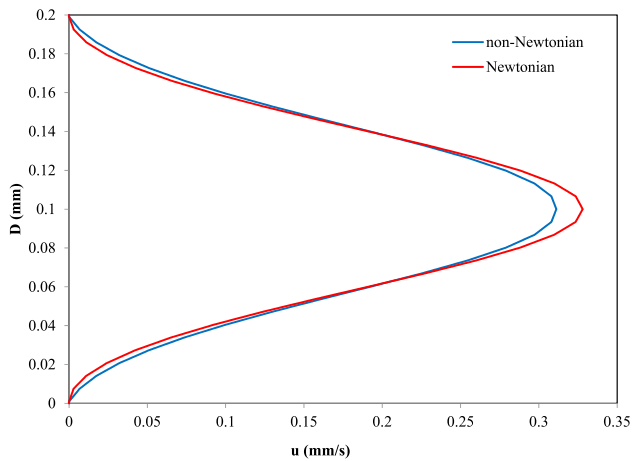


Fig. 14 Blood velocity at the throat for Newtonian and non-Newtonian models

non-Newtonian models are 0.37 mm/s and 0.4 mm/s, respectively. In the case of non-Newtonian fluids, the viscosity is higher compared to Newtonian fluids. As a result, the drag force acting on nanoparticles is greater, leading to higher velocities for the nanoparticles. Consequently, this implies that fewer particles will be captured at the region of interest (ROI).

In Fig. 14, the impact of both Newtonian and non-Newtonian characteristics of blood on the blood velocity at the throat is demonstrated. The figure indicates that the maximum velocity at the throat is approximately 5% greater in the Newtonian model compared to the non-Newtonian model. This disparity arises due to the higher viscosity of blood in the non-Newtonian case, resulting in slower velocity changes. However, the increased viscosity in the non-Newtonian case also leads to a higher drag force acting on the particles, resulting in fewer particles being captured at the ROI.

4 Conclusions

The aim of this research was to investigate the motion and CE of nanoparticles in a blood vessel with stenosis under the influence of a magnetic field. The study examined the impact of various factors such as Reynolds number, nanoparticles diameter, magnetic field strength, Newtonian and non-Newtonian behavior of blood, and magnet type on the CE of nanoparticles in a vessel with local symmetric stenosis. The findings revealed that as the Reynolds number increased, the CE of nanoparticles decreased for all particle diameters. This can be attributed to the higher fluid velocity, resulting in an increased drag force on the nanoparticles, which surpasses the magnetic force and allows the nanoparticles to pass the ROI. Additionally, increasing the magnetic field strength from 0.5 to 1.5 T had a significant effect on the CE for Reynolds numbers of 50 and 100. However, the impact of magnetic field strength was more pronounced for nanoparticles with larger diameters compared to those with smaller diameters. It is crucial to consider blood as a non-Newtonian fluid for small diameter arteries (< 2 mm). The CE of nanoparticles differed by approximately 9% between the Newtonian and non-Newtonian cases for small diameter arteries, whereas the difference was around 1.5% for larger diameter arteries. Based on the obtained results, it is recommended to use a current-carrying wire in vessels with stenosis and a small region of interest. The study also highlighted that future research should focus on investigating the interactions between nanoparticles and particle-particle, as well as particle-red blood cells (RBCs), in the tumor site, along with exploring the arrangement of arrays of current-carrying wires.

Author Contributions Mr. Ardalan has wrote the manuscript and performed the software analysis. Dr. Lahonian and Dr. Aminian have supervised the manuscript and provided the results' analysis. Besides, Mr. Ardalan and Dr. Aminian are responsible for revising the manuscript.

Data Availability The data that support the findings of this study are available on request from the corresponding author.

Declarations

Ethical Approval No human and/or animal tests have been performed.

Research Involving Humans and Animals Statement None.

Conflict of Interest The authors declare no competing interests.

References

- Cherry, E. M., & Eaton, J. K. (2014). A comprehensive model of magnetic particle motion during magnetic drug targeting. *International Journal of Multiphase Flow*, 59, 173–185.

2. Tietze, R., et al. (2015). Magnetic nanoparticle-based drug delivery for cancer therapy. *Biochemical and biophysical research communications*, 468(3), 463–470.
3. Alexiou, C., et al. (2011). Cancer therapy with drug loaded magnetic nanoparticles—magnetic drug targeting. *Journal of Magnetism and Magnetic Materials*, 323(10), 1404–1407.
4. Mohammad-Beigi, H., et al. (2011). Effect of pH, citrate treatment and silane-coupling agent concentration on the magnetic, structural and surface properties of functionalized silica-coated iron oxide nanocomposite particles. *Physica E: Low-dimensional Systems and Nanostructures*, 44(3), 618–627.
5. Rivas, J., et al. (2012). Magnetic nanoparticles for application in cancer therapy. *Journal of Magnetism and Magnetic Materials*, 324(21), 3499–3502.
6. Kempe, H., & Kempe, M. (2010). The use of magnetite nanoparticles for implant-assisted magnetic drug targeting in thrombolytic therapy. *Biomaterials*, 31(36), 9499–9510.
7. Zhang, X., et al. (2010). Chitosan-coated octadecyl-functionalized magnetite nanoparticles: Preparation and application in extraction of trace pollutants from environmental water samples. *Analytical Chemistry*, 82(6), 2363–2371.
8. Borlido, L., Azevedo, A., Roque, A., & Aires-Barros, M. (2013). Magnetic separations in biotechnology. *Biotechnology advances*, 31(8), 1374–1385.
9. Singh, A., et al. (2023). Tailored nanoparticles for magnetic hyperthermia: Highly stable aqueous dispersion of Mn-substituted magnetite superparamagnetic nanoparticles by double surfactant coating for improved heating efficiency. *Journal of Alloys and Compounds*, 976, 172999.
10. Rotariu, O., & Strachan, N. J. (2005). Modelling magnetic carrier particle targeting in the tumor microvasculature for cancer treatment. *Journal of Magnetism and Magnetic Materials*, 293(1), 639–646.
11. Furlani, E., & Ng, K. (2006). Analytical model of magnetic nanoparticle transport and capture in the microvasculature. *Physical review E*, 73(6), 061919.
12. Sharma, S., Katiyar, V., & Singh, U. (2015). Mathematical modelling for trajectories of magnetic nanoparticles in a blood vessel under magnetic field. *Journal of Magnetism and Magnetic Materials*, 379, 102–107.
13. Habibi, M. R., & Ghasemi, M. (2011). Numerical study of magnetic nanoparticles concentration in biofluid (blood) under influence of high gradient magnetic field. *Journal of Magnetism and Magnetic Materials*, 323(1), 32–38.
14. Habibi, M. R., Ghassemi, M., & Hamedi, M. H. (2012). Analysis of high gradient magnetic field effects on distribution of nanoparticles injected into pulsatile blood stream. *Journal of Magnetism and Magnetic Materials*, 324(8), 1473–1482.
15. Stuart, D. C., Kleijn, C., & Kenjereš, S. (2011). An efficient and robust method for Lagrangian magnetic particle tracking in fluid flow simulations on unstructured grids. *Computers & Fluids*, 40(1), 188–194.
16. Sharma, S., Singh, U., & Katiyar, V. (2015). Magnetic field effect on flow parameters of blood along with magnetic particles in a cylindrical tube. *Journal of Magnetism and Magnetic Materials*, 377, 395–401.
17. Shazri, S., & Idres, M. (2017). Numerical investigation of magnetic nanoparticles trajectories for magnetic drug targeting. In *IOP Conference Series: Materials Science and Engineering*. IOP Publishing.
18. Bose, S., & Banerjee, M. (2015). Effect of non-Newtonian characteristics of blood on magnetic particle capture in occluded blood vessel. *Journal of Magnetism and Magnetic Materials*, 374, 611–623.
19. Türk, Ö., Bozkaya, C., & Tezer-Sezgin, M. (2014). A FEM approach to biomagnetic fluid flow in multiple stenosed channels. *Computers & Fluids*, 97, 40–51.
20. Bose, S., & Banerjee, M. (2015). Magnetic particle capture for biomagnetic fluid flow in stenosed aortic bifurcation considering particle–fluid coupling. *Journal of Magnetism and Magnetic Materials*, 385, 32–46.
21. Barnsley, L. C., et al. (2017). Understanding the dynamics of superparamagnetic particles under the influence of high field gradient arrays. *Physics in Medicine & Biology*, 62(6), 2333.
22. de Saint Victor, M., et al. (2017). Magnetic targeting to enhance microbubble delivery in an occluded microarterial bifurcation. *Physics in Medicine & Biology*, 62(18), 7451.
23. Alizadeh, A. A., et al. (2023). Numerical investigation of the injection angle of carrier nanoparticles under the effect of different magnetic fields. *Journal of Magnetism and Magnetic Materials*, 578, 170836.
24. Manshadi, M. K., et al. (2018). Delivery of magnetic micro/nanoparticles and magnetic-based drug/cargo into arterial flow for targeted therapy. *Drug delivery*, 25(1), 1963–1973.
25. Lahonian, M., et al. (2023). Effect of particle–particle and RBC–particle interactions on capture efficiency of magnetic nanocarriers under the influence of a nonuniform magnetic field. *Iranian Journal of Science and Technology, Transactions of Mechanical Engineering*, 1–14.
26. Tzirakis, K., et al. (2014). Numerical investigation of biomagnetic fluids in circular ducts. *International journal for numerical methods in biomedical engineering*, 30(3), 297–317.
27. Ardalan, A., et al. (2021). Effects of geometrical parameters on the capture efficiency of nanoparticles under the influence of the magnetic field in a stenosed vessel. *Powder Technology*, 380, 39–46.
28. Ali, A., et al. (2020). Impact of Lorentz force on the pulsatile flow of a non-Newtonian Casson fluid in a constricted channel using Darcy’s law: a numerical study. *Scientific Reports*, 10(1), 1–15.
29. Davidson, P. A. (2002). *An introduction to magnetohydrodynamics*. American Association of Physics Teachers.
30. Guichard, R., & Belut, E. (2017). Simulation of airborne nanoparticles transport, deposition and aggregation: Experimental validation of a CFD-QMOM approach. *Journal of Aerosol Science*, 104, 16–31.
31. Morsi, S., & Alexander, A. (1972). An investigation of particle trajectories in two-phase flow systems. *Journal of Fluid mechanics*, 55(2), 193–208.
32. Bose, S., et al. (2013). Lagrangian magnetic particle tracking through stenosed artery under pulsatile flow condition. *Journal of Nanotechnology in Engineering and Medicine*, 4(3).
33. Banerjee, M. K., Datta, A., & Ganguly, R. (2010). Magnetic drug targeting in partly occluded blood vessels using magnetic microspheres. *Journal of Nanotechnology in Engineering and Medicine*, 1(4), 041005.
34. Camacho, J., & Sosa, V. (2013). Alternative method to calculate the magnetic field of permanent magnets with azimuthal symmetry. *Revista mexicana de fisica E*, 59(1), 8–17.

Publisher’s Note Springer Nature remains neutral with regard to jurisdictional claims in published maps and institutional affiliations.

Springer Nature or its licensor (e.g. a society or other partner) holds exclusive rights to this article under a publishing agreement with the author(s) or other rightsholder(s); author self-archiving of the accepted manuscript version of this article is solely governed by the terms of such publishing agreement and applicable law.